Resonant cavity LEDs at 655 and 880 nm wavelengths

Pekko Sipilä*, Mika Saarinen, Ville Vilokkinen, Seppo Orsila, Petri Melanen,
Pekka Savolainen, Mika Toivonen, Mihail Dumitrescu, Markus Pessa

Tampere University of Technology, Optoelectronics Research Centre,
P. O. Box 692, 33101 Tampere, Finland

ABSTRACT

Monolithic top-emitting resonant cavity light-emitting diodes (RCLEDs) have been fabricated by solid-source MBE. The RCLEDs in the 650-nm range, with modulation bandwidths exceeding 180 MHz, are possible low-cost transmitter candidates for systems using plastic optical fibers (POFs), such as IEEE-1394 at 100 Mb/s and 200 Mb/s and ATM at 155 Mb/s. Modulation bandwidth of >120 MHz and light power of 2 mW (cw) have been achieved for $^{\varnothing}$84-μm devices driven at a 40 mA current. Accelerated ageing tests for 27,500 device-hours indicate no degradation in output power. A variation in device temperature significantly modifies the far-field pattern and thus the fibre coupling efficiency, due to a cavity detuning effect. The effects of detuning and the temperature and bias dependencies of the devices are investigated. The 880-nm RCLEDs have a maximum output power of 25 mW. Applications include open-air optical communication systems, collision avoidance and measurement systems.

Keywords: Light-emitting diodes, RCLED, MBE, quantum well devices, plastic optical fibers

1. INTRODUCTION

Resonant cavity enhanced light-emitting diodes (RCLEDs) have several interesting properties that make them suitable for various applications, where the usage of conventional LEDs is limited by their poor performance or where edge-emitting laser diodes would be too expensive. RCLEDs present several advantages compared to conventional LEDs such as narrow spectral linewidth, better beam directionality and increased efficiency[1], and higher modulation speed[2]. The enhancements result from the modification of the spontaneous emission by an optical microcavity. Edge-emitting laser diodes require chip-level testing, facet coatings, and precise alignment to an optical fiber, which make them too expensive for many low-level applications. RCLEDs and vertical cavity lasers (VCLs) benefit from their surface-emitting structure which enables wafer-level testing, thus reducing the device fabrication cost in a noticeable degree. Moreover, the circular output beam improves the fiber coupling efficiency.

The RCLED has an optically active region, which consists of quantum wells (QWs) located at antinodes of a standing wave Fabry-Perot cavity mode. The cavity is sandwiched between two distributed Bragg reflectors (DBRs) or between a high-reflectivity metal layer and a DBR mirror. Emission properties of the RCLED can be significantly modified by cavity detuning. Detuning is defined as a difference between the Fabry-Perot mode λ_{FP} and the quantum well emission λ_{qw}; i.e., $\Delta\lambda_d = \lambda_{FP} - \lambda_{qw}$. A positive detuning increases the extraction efficiency (η_e) and output power (P_{out}), and broadens the far-field (FF) distribution[3]. When compared to a VCL, the RCLED has favorable structural features: the top DBR needs not be of very high reflectivity ($80 < R_t < 90$ % is adequate), and the window area may be large to yield a good extraction efficiency. Therefore, medium-speed high-brightness RCLEDs can be designed for a wide spectral range, including visible light where lasing action of vertically emitting devices is difficult to be achieved[4,5,6].

A driving force of our RCLED studies is the market introduction of polymethyl methacrylate (PMMA) polymer optical fibers (POFs). PMMA-POF, exhibiting a data transmission window at $\lambda \approx 650$ nm, is suitable for low-cost short-haul communications systems[7]. Due to its large core diameter ($0.1 \le \varnothing \le 3.0$ mm), POF can easily be aligned and terminated. However, light propagation losses are high, typically 0.15 - 0.20 dB/m at the optimal wavelength. Another drawback of the POF technology is the absence of a low-cost, high performance light source. In principle, an LED could be used as a transmitter but it would produce a narrow modulation bandwidth (f_t), typically $20 < f_t < 30$ MHz, and broad emission of 20 to 30 nm in terms of full width at half maximum ($FWHM$). An edge-emitting laser, in turn, would allow for large f_t, but

* Correspondence: Email: pekko.sipila@orc.tut.fi; Telephone: +358 3 365 2552; Fax: +358 3 365 3400

In *Light-Emitting Diodes: Research, Manufacturing, and Applications IV*, H. Walter Yao, Ian T. Ferguson, E. Fred Schubert, Editors, Proceedings of SPIE Vol. 3938 (2000) • 0277-786X/00/$15.00

would be expensive and its high-temperature behaviour — a key issue particularly in automotive applications — is not well known. Bearing these difficulties in mind, a cost-effective medium-speed RCLED may be a viable device for POF-based communication systems.

In this paper, we will describe our work on RCLEDs at 650-655 nm and 880 nm wavelengths. Design issues, experimental procedures and device performance will be discussed. Because of their more obvious applications, the main focus here will be on the red RCLEDs.

2. DESIGN ISSUES

We have studied several kinds of RCLED structures in order to optimize the device performance. The basic structure consisted of a cosine-type 1-λ-thick cavity delimited by AlGaAs DBR mirrors and having an active region (with 3 to 5 QWs) centred at the cavity antinode. The cavity thickness was designed to be $L_c = m_c\lambda_{FP}/2n$, where λ_{FP} is the wavelength in the outside medium, n is the refractive index of the cavity material, and m_c is the cavity order ($m_c = 2$ for a 1-λ cavity). Top emission was considered because of the GaAs substrate absorption in the working spectral ranges and monolithic structures were chosen since they enable integration and have reduced fabrication complexity.

Transfer matrix based modeling together with a self-consistent model were used to optimise the devices' performance. The design of the layer structure (DBRs, microcavity, QWs, barriers, current spreading and cap layers) and doping profile was assisted by computer simulations that enabled many device improvements.

In a first modeling and simulation step the QW composition and thickness together with the barrier thickness were chosen, using a self-consistent model, so that the resulted spontaneous emission spectrum is peaked at the desired wavelength. The self-consistent model uses interband transition; strained QWs are treated using the k·p theory and valence band mixing effects are included. It has to be mentioned that since the spontaneous emission spectrum depends strongly upon bias and temperature while the active region temperature and the relation between injected current and QW carrier densities (used in the model) are highly uncertain, the calculated spontaneous emission spectrum must be fitted to measurements.

Once the cavity was defined, the bottom and top DBRs were designed. Besides a desired large refractive index contrast Δn, one should achieve low photon absorption and small potential barriers between individual layers. Unfortunately, high contrast in AlGaAs layers is limited in the red range by significant absorption at reduced aluminum content.

Since the devices' electrical characteristics are as much important as the optical ones an electrical analysis was performed in conjunction with the optical analysis. The absorption edge's (bandgap) and potential barriers' variation with layer composition, layer thickness and bias were analyzed at this stage with the aid of the self-consistent model. In order to alleviate the adverse effects of the DBR potential barriers, intermediate-composition barrier reduction layers were used before each high bandgap material layer (in the direction of majority carrier flow). The composition and thickness of the intermediate DBR layers were adjusted by analyzing the band profile calculated with the self-consistent model. The resulted optimum composition was roughly in the middle of the composition gap between low and high bandgap layers. In order to keep the optical properties of the mirrors unaffected the intermediate composition layer thickness was kept much smaller than the emission wavelength. The thickness of the high bandgap layer was adjusted so that the optical thickness of the combined intermediate composition and high bandgap layer is $\lambda_0/4$.

Also in order to improve the electrical device characteristics of the 650-nm RCLEDs the bottom DBR was made of N instead of the typical N+½ periods, starting with low bandgap (high refraction index) layer on the substrate side. This was done since the GaAs to low-bandgap material interface produces a favorable barrier reduction step for electrons. The number of periods in the bottom mirror was high enough, so that the contrast at the interface with the GaAs substrate is not important from the optical point of view. In a similar attempt to introduce a barrier reduction step at the first potential barrier for holes the current spreading layer was made of low bandgap (high refraction index) material.

The reflection coefficients of the DBRs were calculated using a transfer-matrix-based program[8]. The optical analysis of the RCLED layer structure is very much based on the determination of the reflectivity dependence upon wavelength, incidence angle, polarization, layer contrast, layer thickness, and the number of DBR periods. Once the DBR layer composition, order and thickness are established the remaining variable to adjust the DBR mirror reflectivities is the number of periods. For top-emitting structures, the bottom DBR should have a reflectivity close to unity. We chose a 20-period

$Al_{0.9}Ga_{0.1}As/Al_{0.2}Ga_{0.8}As$ bottom DBR for the 880-nm RCLEDs and a 32-period $AlAs/Al_{0.5}Ga_{0.5}As$ bottom DBR with $Al_{0.75}Ga_{0.25}As$ intermediate composition layers for the 650-nm RCLEDs, giving calculated reflectivities of 98 and 99 % at normal incidence, respectively. The top mirror reflectivity must be adjusted to significantly lower values – so that the cavity modes over the whole emission spectrum occupy as much as possible of the escape window. For lateral current confinement, an $Al_{0.98}Ga_{0.02}As$ wet thermal oxidation layer was placed in the top DBR, one period away from the cavity in order to avoid oxide modes and strain propagation into the cavity. Ion implantation could also be used for current confinement, with the advantage of maintaining planar device structure. However, ion implantation used in VCL fabrication has been reported to deteriorate device reliability by introducing crystalline defects that propagate into the device's active region[9].

In order to optimize the extraction efficiency the DBR mirrors and the cavity must be detuned with respect to the emission spectrum peak. Unfortunately, a trade-off must be made between extraction efficiency and directionality. The extraction efficiency is at maximum when the cavity mode is centered in the middle of the escape window, corresponding to an double-lobed *FF* with maxima at an angle of $\theta \approx 45°$ off the surface[3]. On the other hand, such a large θ is not desired for optical fiber coupling experiments. Detuning allows the *FF* to be optimized according to the application. The effect of detuning on the *FF* can be seen in figure 1, which shows the measured far-fields for three 650-range RCLEDs with different detunings.

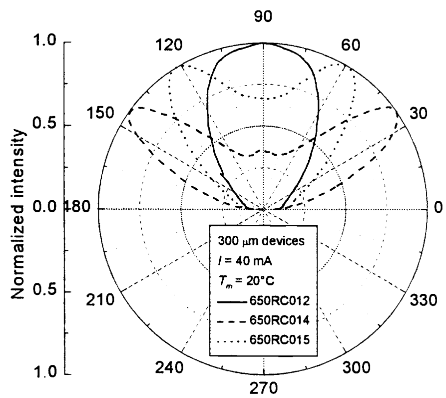

Figure 1 Measured far-field patterns for three RCLEDs in the 650-nm range with different nominal detunings: $\Delta\lambda_d$(650RC012) $\approx$ 0nm, $\Delta\lambda_d$(650RC015) $\approx$ 6nm, $\Delta\lambda_d$(650RC014) $\approx$ 14nm

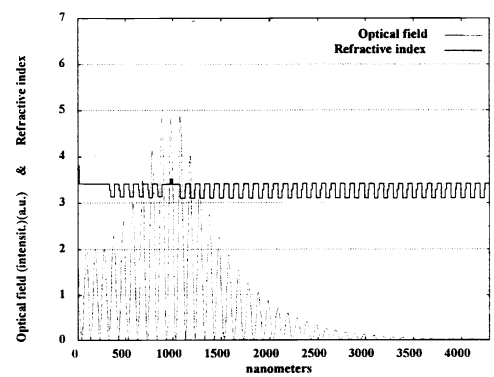

Figure 2 Refractive index and optical field intensity profiles along a 1-λ cosine cavity RCLED.

Based on the transfer matrix formalism the study of optical field longitudinal distribution enabled us to analyse the QW placement and evaluate doping profiles to reduce the free carrier absorption. Figure 2 shows the refractive index and the optical field profile for a 1-λ cosine-cavity 650-nm RCLED. Only one of the QWs can be placed at the single antinode available; the additional QWs being less effectively coupled with the cavity mode. The optimum number of QWs is odd – to have one QW placed exactly at the antinode – and in the range of 3 to 7 depending on the QW and barrier thickness. Higher number of QWs induces reduced and non-uniform carrier injection into the QWs besides bad coupling to the cavity mode for the QWs farther from the antinode.

3. GROWTH AND DEVICE PROCESSING

All our RCLED structures were grown on 2" GaAs wafers by solid-source MBE[10] using valved cracker cells for arsenic and phosphorous. Silicon and beryllium were used as *n*- and *p*-type dopants, respectively. Prior to the growth of the device structures, test samples were grown to adjust the stop-band of the DBRs, and for photoluminescence (PL) studies.

The 650-nm RCLED structure consisted of a 32 period *n*-doped $Al_{0.5}Ga_{0.5}As/AlAs$ bottom DBR mirror (with $Al_{0.75}Ga_{0.25}As$ intermediate composition layers), a 1-λ cosine cavity with 3 to 5 $In_{0.55}Ga_{0.45}P$ QWs and $(Al_{0.5}Ga_{0.5})_{0.51}In_{0.49}P$ barriers and semicavities, a 5 to 12 period p-doped $Al_{0.95}Ga_{0.05}As/Al_{0.5}Ga_{0.5}As$ top DBR mirror (also with $Al_{0.75}Ga_{0.25}As$ intermediate composition layers) having an $Al_{0.98}Ga_{0.02}As$ wet thermal oxidation layer in the second period from the cavity and an $Al_{0.5}Ga_{0.5}As$ current spreading layer with a thin p^{++} GaAs contact layer on top.

The 880-nm RCLED structure consisted of a 20 period n-doped $Al_{0.2}Ga_{0.8}As/Al_{0.9}Ga_{0.1}As$ bottom DBR mirror, a 1-λ cosine cavity with three $In_{0.04}Ga_{0.96}As$ QWs, $Al_{0.2}Ga_{0.8}As$ barriers and semicavities and a 5 to 7 period p-doped $Al_{0.9}Ga_{0.1}As/Al_{0.2}Ga_{0.8}As$ top DBR mirror with an $Al_{0.97}Ga_{0.03}As$ wet thermal oxidation layer. On top a thick $Al_{0.2}Ga_{0.8}As$ current spreading layer with a p^{++} GaAs contact layer was grown. No barrier reduction layers were used in the 880-nm RCLEDs.

The samples were processed into circular top-emitting mesas with emission window diameters of $40 \leq \varnothing \leq 500$ μm. To enhance the current distribution over the window area, 3-10 μm wide contact stripes crossed the circular emission window. The oxide aperture for lateral current confinement was formed by a wet thermal oxidation step at 375-400 °C. The p-type metal contact, Ti/Pt/Au, was made on the mesas by e-beam evaporation and standard lift-off. The n-type contact, Ni/Au/Ge/Au, was evaporated on the backside of a thinned (100 μm) substrate. Finally, the GaAs contact layer was removed from the window area by wet selective etching to avoid light absorption. The devices were bonded on TO-46 cans with silver filled epoxy. Some of the devices were encapsulated in transparent epoxy to enhance light extraction through decreased refractive index contrast at the semiconductor/air interface.

4. RESULTS AND DISCUSSION

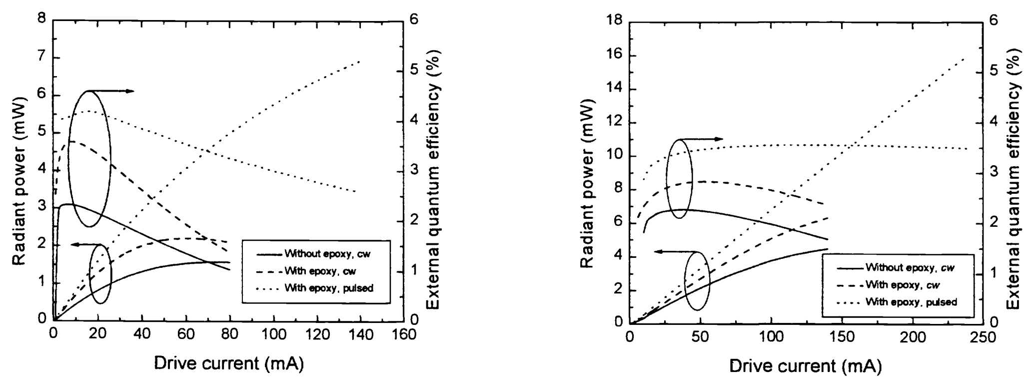

Figure 3 Radiant power and external quantum efficiency for a 650-nm RCLED having an $^{\varnothing}$84-μm (left) and a $^{\varnothing}$300-μm (right) emission window without an epoxy cap in cw mode, and with an epoxy cap in cw mode and in pulsed mode.

Figure 3 shows light-current-external quantum efficiency (L-I-η) curves for 650-nm RCLEDs having an $^{\varnothing}$84-μm and a $^{\varnothing}$300-μm emission window with and without transparent epoxy caps. The curves were measured at the device temperature (T_m) of 20 °C, defined as a temperature of the TO-46 mount, using an integrating sphere and a calibrated optical spectrometer. The $^{\varnothing}$84-μm devices turned on at bias voltage $1.7 \leq V_b \leq 1.8$ V and had a differential series resistance of 3 Ω at drive current $I_{dr} = 50$ mA. According to figure 3, P_{out} saturated at about 1.6 mW (cw) for a chip with no epoxy cap, due to internal heating, and at 2.2 mW (cw) for a chip with the cap. Maximum η of about 2.3 % and 3.6 % for the device without and with the epoxy cap, respectively, was achieved at $I_{dr} \approx 8$ mA. The power values are somewhat smaller than reported by Streubel *et al.* for MOCVD-grown devices of the same size that had a hydrogen ion implanted current confinement structure[6]. However, our devices with the barrier reduction layers in the DBRs have a slightly smaller forward voltage and a lower differential series resistance. Since detrimental effects of heating on P_{out} (cw) were remarkable, we measured P_{out} in pulsed mode as well (pulse width = 2 μs, duty cycle = 2.5 %), as shown in figure 3. We obtained $P_{out} \approx 7$ mW at $I_{dr} = 140$ mA with no remarkable indication of thermal saturation. For the $^{\varnothing}$300-μm devices, the external quantum efficiency remains smaller, the maximum being 2.8 % for the epoxy-capped component in cw mode. Due to the larger contact area, the differential series resistance for the larger device size is smaller, only 1.2 Ω.

The performance curves in cw mode for 880-nm RCLEDs having ∅80-μm and ∅500-μm emission windows and an epoxy cap are shown in figure 4. The maximum external quantum efficiencies are >16 % and 14 %, respectively. These values are similar to the efficiencies reported by other groups for near-IR RCLEDs, such as 14.8 % by Dill *et al.*[11] for a 960-nm RCLED (pulsed measurement), and 19.8 % for a ∅1.5 mm and 16.8 % for an ∅85-μm RCLED by De Neve *et al.* at 980 nm[12]. The voltage and the series resistance are significantly higher than for the red RCLEDs with the barrier reduction layers.

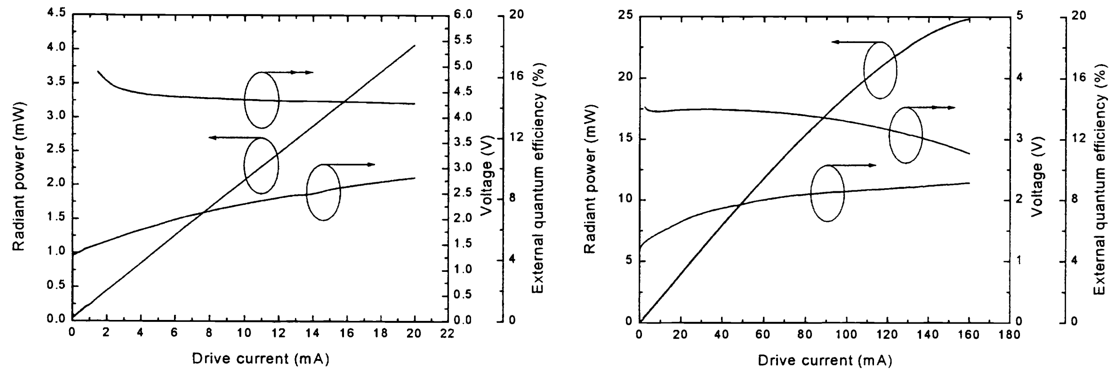

Figure 4 Radiant power, forward voltage and external quantum efficiency in cw mode for 880-nm RCLED having an ∅84-μm (left) and a ∅500-μm (right) emission window.

The spectrum for an 880-nm RCLED together with a commercial reference LED is shown in figure 5. When talking about the spectral properties of an RCLED, one should note that in contrast to conventional LEDs, the RCLEDs show angular wavelength dispersion caused by the resonant cavity[3]. Consequently, the peak wavelength and the *FWHM* depend both on θ and on the solid angle inside which the light is collected. The spectra in figure 4 are measured using an integrating sphere, thus collecting all the light emitted by the devices. If a fiber with a small numerical aperture would be used instead, a much smaller *FWHM* would be measured for the RCLED.

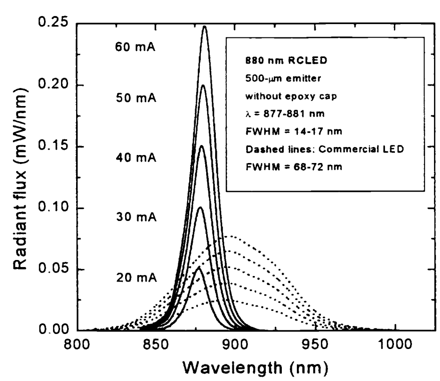

Figure 5 Electroluminescence spectra for an 880-nm RCLED and a commercial LED.

An increase in T_m caused a line shift ($\Delta\lambda$) in λ_{qw} and λ_c towards longer wavelengths. This red-shift was due to thermal expansion of the crystal lattice and a concomitant decrease in band gap, which lowered the energy states of the quantum well and broadened the cavity. The quantum well emission was shifted more than the cavity mode, forcing $\Delta\lambda_d \rightarrow 0$ nm and leading to single-lobed emission normal to the exit window.

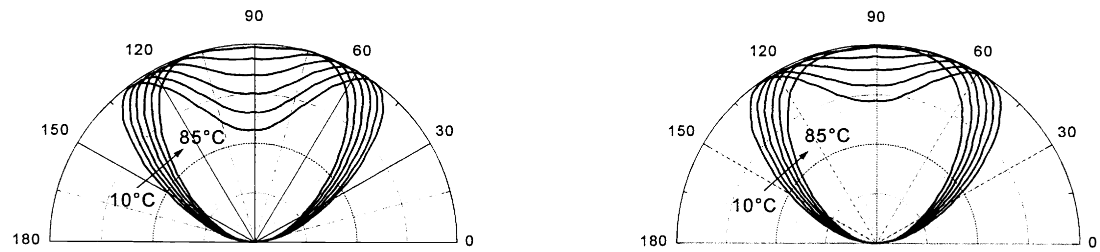

Figure 6 Far-field pattern of an 650-nm RCLED at I_{dr} = 10 mA (left) and I_{dr} = 40 mA (right) as a function of device temperature (10 ≤ T_m ≤ 85 °C, 15 °C step). The emission cone becomes remarkably narrower, as temperature is increased, improving the coupling of light into an optical fibre.

Figure 6 shows the evolution of *FF* for a 650-nm RCLED with an $^{\varnothing}$84-μm window in the temperature interval 10 ≤ T_m ≤ 85 °C when I_{dr} = 10 and 40 mA, respectively. For low T_m = 10 °C, where $\Delta\lambda_d$ >> 0 nm, emission takes place preferably at the angle of ±32° for I_{dr} = 10 mA and ±37° for I_{dr} = 40 mA, while for T_m = 85 °C the angle of the lobe is zero for both drive currents. The narrower angle at higher current is a consequence of internal heating. The exact resonance at normal emission reduces η_e, which is not desired for high-T_m applications, as noted previously. Nevertheless, the fact that *FF* is a function of T_m and can vary tens of degrees is very useful. This is because the narrowing of *FF* at high T_m improves the fibre coupling efficiency and offsets, in part, a decrease in P_{out}.

This is shown in figure 7, where the output power and coupling efficiency determined for emission from the end of a fibre (1 m long 0.98 / 1.00 mm PMMA-POF, *NA* = 0.5) at I_{dr} = 10–40 mA is presented. To couple the light into the fibre, a $^{\varnothing}$84-μm device having neither epoxy nor a collimating lens was placed on the optical axis of the fibre, with an air gap of ~1 mm between the fibre and the device. The temperature coefficient (*TC*) describing a change in P_{out} varies from –0.72 for I_{dr} = 10 mA to –0.89 %/°C for I_{dr} = 40 mA in the range 10 < T_m < 85 °C. Our devices having wider far-fields (θ ~50°) exhibited somewhat smaller *TC*, -0.50 and -0.83 %/°C at the aforementioned currents, respectively, but due to the wider *FF* the coupling efficiency was poorer. All these *TC*s are probably too large for cost-effective POF-based data transmission systems. Therefore, a new cavity design is needed; otherwise, the system would require a receiver with a large dynamic range or a transmitter with a Peltier cooler, both solutions being expensive.

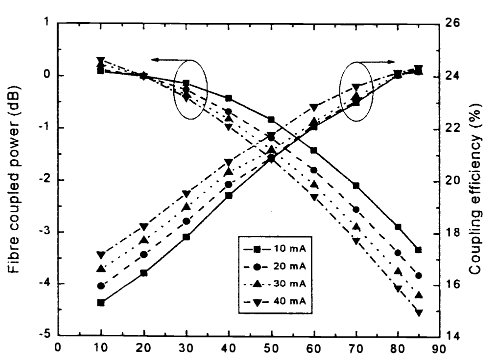

Figure 7 Fibre-coupled power (with respect to the power at 20 °C) and coupling efficiency at four different drive currents as a function of device temperature. Fibre: 0.98/1.00 mm PMMA step-index POF, NA = 0.5.

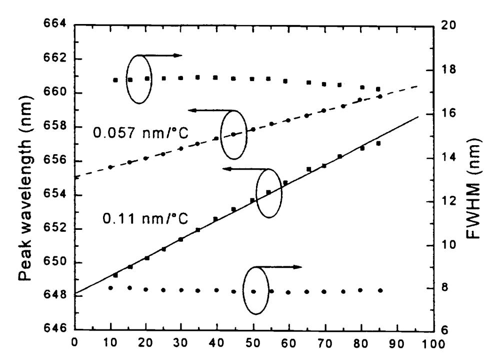

Figure 8 Peak wavelength and *FWHM* for emission into free space (■) and for emission from the end of a POF (●).

Figure 8 displays λ and *FWHM* plotted against T_m for emission into free space and for emission from the exit of a 1-m long fibre. The fibre-coupled spectrum exhibits longer λ. This is because of the resonant θ - λ dispersion relation, and because emission normal to the surface (with the longest λ) is best coupled into the fibre. The temperature gradient is reasonable, only +0.11 nm/°C and +0.057 nm/°C for the two cases, respectively. The *FWHM* shows very stable temperature behavior in both cases.

Dynamic properties were studied using a network analyser, a 3 GHz bias-tee, and a Si detector equipped with a low-noise amplifier and free-space collimation optics. The detector had a modulation bandwidth of 1 GHz. To avoid the signal saturation at low bias, we used a *rf* modulation signal power of -15 dBm at I_{dr} < 20 mA. At higher currents, a *rf* power of -5 dBm was applied.

Figure 9 shows room-temperature $f_{t,-3dB}$ as a function of I_{dr}. The bandwidth increased almost linearly with I_{dr}, being about 85 - 100 MHz at 15 - 20 mA and 180 MHz at 80 mA. This dependence of $f_t = f_t(I_{dr})$ can be accounted for by two major effects. Namely, it is known that the input impedance decreases, as I_{dr} is increased (this effect is important at low bias) and, secondly, the carrier lifetime decreases as the current density increases[14]. Adding an epoxy cap improved f_t by about 10 %, this improvement being due to enhanced heat conduction.

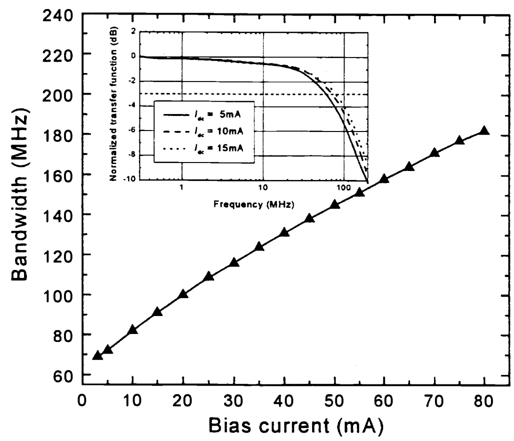

Figure 9 Modulation bandwidth of an $^{\varnothing}$84-μm RCLED as a function of *dc* bias current. Inset shows transfer functions at three different bias currents.

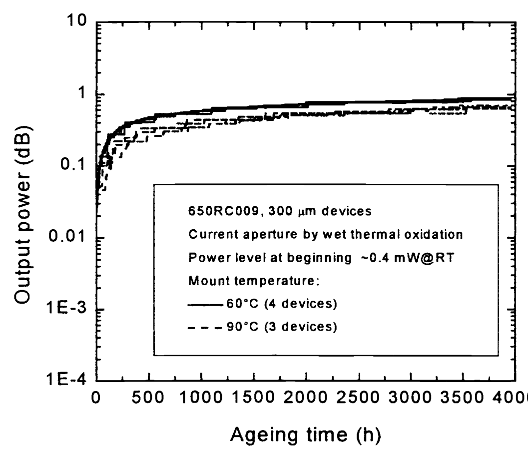

Figure 10 Accelerated ageing tests for nine $^{\varnothing}$300-μm devices in a constant current mode. Neither a sudden failure nor any degradation has taken place during 27,500 device-hours on test.

Finally, we present reliability features of RCLEDs as deduced from preliminary experiments. Accelerated ageing tests on nine $^{\varnothing}$300-μm devices were carried out in a constant current mode at 60 °C and 90 °C at initial P_{out}(20 °C) ≈ 0.4 mW. The results are shown in figure 10. No sudden unexpected failure has occurred during 27,500 device hours on test. In fact, the devices still exhibit a slight improvement in output power, likely due to a residual burn-in effect with a related reduction in non-radiative carrier traps in the quantum wells.

5. SUMMARY

We have fabricated MBE-grown, monolithical RCLEDs emitting in the 650-nm range and at 880 nm. The 650-nm RCLEDs, with measured modulation bandwidth of 180 MHz, are possible low-cost transmitter candidates for systems using plastic optical fibers (POF), such as IEEE-1394 at 100 Mb/s and 200 Mb/s and ATM at 155 Mb/s. For these devices, good beam directionality ensures efficient fiber coupling. A small temperature dependence of peak wavelength, 0.057 nm/°C, and a nearly temperature independent *FWHM* of ~8 nm were observed for POF-coupled emission. The 880-nm RCLEDs had a maximum output power of 25 mW (cw). Applications include open-air optical communication systems, collision avoidance and measurement systems. The effects of detuning on beam directionality and coupling efficiency were demonstrated. Also, the temperature and bias dependences of the devices were investigated. It was shown that increase in device temperature significantly improves the coupling efficiency into an optical fiber. Preliminary ageing tests show very good reliability for the devices with an oxidized current aperture.

ACKNOWLEDGMENTS

This work was supported, in part, by a European Union research project (SMILED) and a Finnish national research project (SUPREME).

REFERENCES

1. E. F. Schubert, Y.-H. Wang, A. Y. Cho, L.-W. Tu, and G. J. Zydzik, "Resonant cavity light-emitting diode," *Appl. Phys. Lett.*, **60**, pp. 921-923, 1992.
2. E. F. Schubert, N. E. J. Hunt, R. J. Malik, M. Micovic, and D. L. Miller, "Temperature and modulation characteristics of resonant-cavity light-emitting diodes," *J. Lightwave Technol.*, **14**, pp. 1721-1729, 1996.
3. H. Benisty, H. De Neve, and C. Weisbuch, "Impact of planar microcavity effects on light extraction – Part I: Basic concepts and analytical trends," *IEEE J. Quantum Electron.*, **34**, pp. 1612-1631, 1998.
4. J. A. Lott, R. P. Schneider, Jr., J. C. Zolper, K. J. Malloy, "AlGaInP visible resonant cavity light-emitting diodes," *IEEE Photon. Technol. Lett.*, **5**, pp. 631-633, 1993.
5. M. Jalonen, J. Köngäs, M. Toivonen, P. Savolainen, A. Salokatve, and M. Pessa, "Monolithic super-bright red resonant cavity light-emitting diode grown by solid source molecular beam epitaxy," *IEEE Photon. Technol. Lett.*, **10**, pp. 923-925, 1998.
6. K. Streubel, U. Helin, V. Oskarsson, E. Bäcklin, and Å. Johansson, "High brightness visible (660 nm) resonant-cavity light-emitting diode," *IEEE Photon. Technol. Lett.*, **10**, pp. 1685-1687, 1998.
7. T. Ishigure, M. Satoh, O. Takanashi, E. Nihei, T. Nyu, S. Yamazaki, and Y. Koike, "Formation of the refractive index profile in the graded index polymer optical fiber for gigabit data transmission," *J. Lightwave Technol.*, **15**, pp. 2095-2100, 1997.
8. M. Dumitrescu, P. Sipilä, V. Vilokkinen, L. Toikkanen, P. Melanen, M. Saarinen, S. Orsila, P. Savolainen, M. Toivonen, and M. Pessa, "Resonant cavity light-emitting diodes: modeling, design and optimization", SIOEL'99, SPIE 6th Symp. on Optoelectronics, Bucharest, Romania, 22-24 Sept. 1999.
9. W. Jiang, C. Gaw, P. Kiely, B. Lawrence, M. Lebby, and P. R. Claisse, "Effect of proton implantation on the degradation of GaAs/AlGaAs vertical cavity surface emitting lasers", *Electronics Letters*, **33**, pp. 137-139, 1997.
10. M. Pessa, M. Toivonen, M. Jalonen, P. Savolainen, and A. Salokatve, "All-solid-source molecular beam epitaxy for growth of III-V compound semiconductors," *Thin Solid Films,* **306**, pp. 237-243, 1997.
11. C. Dill, R. P. Stanley, U. Oesterle, D. Ochoa, and M. Ilegems, "Effect of detuning on the angular emission pattern of high-efficiency microcavity light-emitting diodes", *Appl. Phys. Lett.*, **73**, pp. 3812-3814, 1998.
12. H. De Neve, J. Blondelle, P. Van Daele, P. Demeester, R. Baets, and G. Borghs, "Recycling of guided mode light emission in planar microcavity light emitting diodes", *Appl. Phys. Lett.*, **70**, pp. 799-801, 1997.
13. G. E. Shtengel, D. A. Ackerman, and P. A. Morton, "True carrier lifetime measurements of semiconductor lasers," *Electron. Lett.*, **31**, pp. 1747-1748, 1995.